

Functionally Graded AA7075 Components Produced via Hot Stamping: A Novel Process Design Inspired from Analysis of Microstructure and Mechanical Properties

Ezgi Bütev Öcal,* Seyed Vahid Sajadifar, Erik P. K. Sellner, Malte Vollmer, Akbar Heidarzadeh, Janez Zavašnik, Thomas Niendorf, and Peter Groche

Herein, functionally graded AA7075 components manufactured via hot stamping are investigated by focusing on the effect of different process variables on localized microstructure evolution. To realize gradation through stamping, an active tool is designed and applied. The design of experiments allows to assess the impact of transfer time from the furnace to the tool, quenching time in the tool, and final quenching media. Related characteristics of mechanical properties throughout the hat-shaped profile are assessed via hardness and tensile tests. As expected, the sections of the samples formed in the cooled part of the tool are characterized by higher mechanical strength following subsequent aging, while sections formed in the heated part exhibit higher ductility. Moreover, the microstructural analysis reveals that fine precipitates with minimum interparticle distances only form in the cooled section of the samples. Increasing the tool temperature at the heated side to 350 °C results in the formation of coarse precipitates in the grain interior and along the grain boundaries. A sharp gradient in terms of microstructural and mechanical properties is found between these conditions. After reducing the transfer time, an increased volume fraction of fine precipitates leads to further improvements in hardness and mechanical strengths.

their high strength-to-weight ratio, excellent structural performance, and good corrosion resistance. However, their limited formability and high springback at room temperature restrict further applications. As a result, several temperature-assisted forming processes have been developed, either softening the material for cold forming through an appropriate pretreatment^[1,2] or using elevated forming temperatures.^[3–8] Quite recently, a hot forming–quenching (HFQ) integrated process has been developed by Jiang et al. for forming high-strength Al alloys.^[4] The basic principle is to finalize the forming process before any aging-induced strengthening. Clearly, such an approach can be exploited to reduce the springback and increase formability.

Increasing passenger safety standards in the automotive sector requires improved performance crash structures. In the case of components made of steel, adapted processing procedures have been developed throughout the last decades. High-performance crash components can be

1. Introduction


High-strength aluminum alloys such as AA7075 are widely used in the mobility sector to meet the need for improved energy efficiency through lightweight design. Here, major advantages are

achieved with graded properties, combining high strength areas with areas of high energy absorption in the same part. The tailored tempering process is one of the manufacturing strategies to obtain these functionally optimized properties. The tailored properties are achieved by controlling the cooling conditions during

E. Bütev Öcal, E. P. K. Sellner, P. Groche
Institute for Production Engineering and Forming Machines
Technical University of Darmstadt
64287 Darmstadt, Germany
E-mail: ezgi.oecal@ptu.tu-darmstadt.de

S. V. Sajadifar, M. Vollmer, T. Niendorf
Institute of Materials Engineering
University of Kassel
34125 Kassel, Germany

A. Heidarzadeh
Department of Materials Engineering
Azarbaijan Shahid Madani University
Tabriz 53714-161, Iran

 The ORCID identification number(s) for the author(s) of this article can be found under <https://doi.org/10.1002/adem.202201879>.

J. Zavašnik
Department Structure and Nano- / Micromechanics of Materials
Max-Planck-Institut für Eisenforschung
40237 Düsseldorf, Germany

© 2023 The Authors. Advanced Engineering Materials published by Wiley-VCH GmbH. This is an open access article under the terms of the Creative Commons Attribution-NonCommercial License, which permits use, distribution and reproduction in any medium, provided the original work is properly cited and is not used for commercial purposes.

J. Zavašnik
Gaseous Electronics
Jožef Stefan Institute
1000 Ljubljana, Slovenia

DOI: 10.1002/adem.202201879

the forming and quenching process.^[9–15] Tang et al. designed segmented dies with active heating via heating cartridges and active water cooling to nearly room temperature.^[12] They found that the final properties of the formed 22MnB5 steel part can be controlled by tailored tempering, in which hardness changes between heated and cooled zones are observed. Similarly, George et al. produced a laboratory-scale B-pillar Usibor 1500P boron steel employing heated and cooled tooling, which can control the cooling rate locally to obtain crash-optimized tailored properties in the same part.^[13]

A similar process was employed for aluminum alloys. Sajadifar et al. performed a hot stamping–quenching process for AA6082 and AA7075 at varying cooling rates through different tool temperatures to investigate the changes in the final microstructures.^[6,16] They observed that the change in the tool temperature influences the quenching rate. A higher quenching rate promotes the formation of fine precipitates during aging treatment by creating a well-defined supersaturated solid solution (SSSS) state before. Fan et al. examined the hot forming–quenching process for 6A02 aluminum alloy in terms of microstructural and mechanical properties.^[3] They found that the optimum tool temperature is 250 °C to obtain optimized strength and formability simultaneously. Scharifi et al. presented similar findings using various tool temperatures between 100 and 350 °C for the hot stamping process of AA6082 and AA7075 alloys. No significant changes were seen in the strength of the alloys for tool temperatures up to 200 °C.^[17] A further increase to 350 °C decreased the yield and ultimate tensile strength while increasing the elongation continuously with increasing tool temperature. Therefore, it can be concluded that specific local material properties in the high strength solution heat treated (SHT) aluminum alloys can be adjusted by hot forming with a controlled cooling rate during tool quenching.^[6,18]

In the literature available so far, only a very limited number of studies provide details on local modification of properties of AA7xxx series aluminum alloys.^[19,20] To tackle this research gap, the present study was conducted. The comprehensive study detailed in the remainder of the article concentrates on obtaining graded properties throughout the formed hat-shaped profile by controlling the cooling conditions during the hot stamping process. Thermomechanically processed AA7075 alloy sheets following different forming–quenching times are examined to understand the effect of various parameters on the final strengthening behavior. Moreover, the effect of different transfer times, which play a key role in the resulting properties, was also investigated. The microstructure evolution and strengthening mechanism were analyzed by scanning electron microscopy (SEM), transmission electron microscopy (TEM), and X-ray diffraction (XRD) analysis. The mechanical properties of the profile are investigated via Vickers microhardness and uniaxial tensile test. Results obtained are used to highlight future challenges toward the development of high-strength aluminum alloys with graded properties that can be used in the automotive industry.

2. Experimental Section

2.1. Material

The material used in the present study is AA7075 alloy in T6 condition supplied from AMAG rolling GmbH. The sheets had a thickness of 1.5 mm. The chemical composition reported by the manufacturer is given in **Table 1**. The sheets were cut to blanks of 260 × 200 × 1.5 mm³. In order to decrease adhesion effects at the high forming temperatures, the blanks were coated with Mechano-Lube 6VP813 lubricant applied by a spray gun

Table 1. Chemical composition of AA7075 alloy.

Chemical composition [wt%]									
Si	Fe	Cu	Mn	Mg	Cr	Zn	Ti	Ti + Zr	Al
Max. 0.40	Max. 0.50	1.2–2.0	Max. 0.30	2.1–2.9	0.18–0.28	5.1–6.1	0–0.20	Max. 0.25	Balance

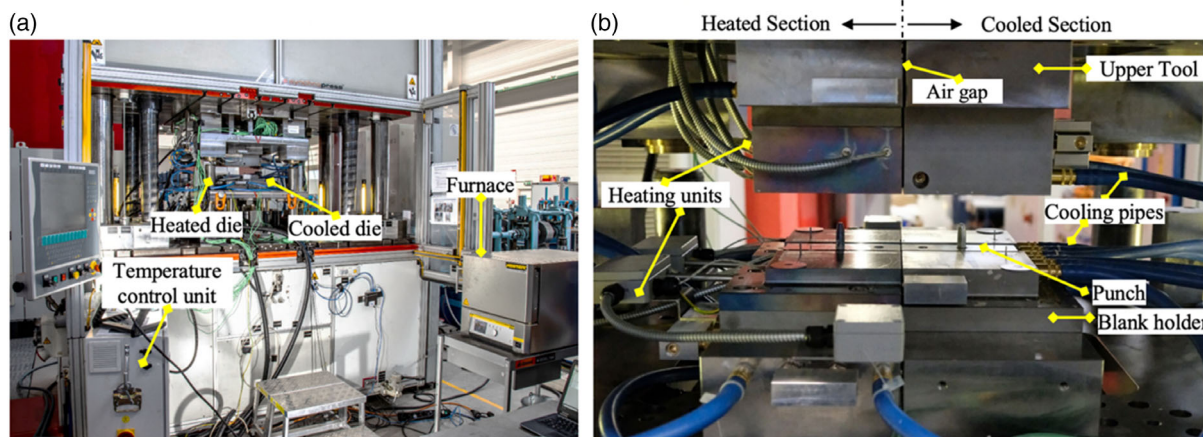


Figure 1. a) Experimental setup for the hot stamping process, and b) details of the active tool parts.

before hot stamping. The tool material used was Uddeholm Unimax tool steel hardened to 57 HRC.

2.2. Hot Stamping

Hot stamping experiments were conducted by using a specifically designed tool depicted in **Figure 1a** to control the tooling temperature as well as the resulting properties of the hat-shaped profile. Graded properties were to be set via differential cooling conditions in the same tool during the hot stamping process. As shown in **Figure 1b**, one side of the tool is actively heated by electrical heating components to a set temperature in a closed loop control. In all tests, a homogeneous temperature distribution was achieved. The other side of the tool is cooled by water flow through channels. Heat transfer at the parting plane of the segmented tool is limited by a 2 mm air gap in the tools (**Figure 1b**). The drawing depth was set to 40 mm for hot stamping. A constant distancing of 1.7 mm was maintained between the upper and lower tools. K-type thermocouples (TCs) were inserted into both heated and cooled tools to measure the temperature evolution during the process.

The schematic representation of the hot stamping process is shown in **Figure 2**. The blank was SHT at 480 °C for 15 min and then transferred to the forming tool with different transfer times. It was placed on spring-suspended pins at a distance of 10 mm from the tool surface to reduce heat transfer before forming. During the combined forming and quenching stage, the hat-shaped profile was formed, and a heat transfer between the blank and the tool occurred. After a specific quenching time in the tool, the part was extracted and cooled down before applying aging at 120 °C for 20 h. A Nabertherm NA 15/65 furnace was used for the SHT and the aging process. The temperatures of the heated tools, the SHT, and aging conditions were defined based on the study by Sajadifar et al.^[16] The temperature of the cooled tool section was kept constant at around room temperature, while the heated tool section was kept at 350 °C for all experiments. Different process parameters, i.e., transfer times (25 and 10 s), quenching times in the tool (8 and 30 s), and cooling media (air and water), **Table 2**, were applied to assess their influence on the characteristics of the transition area and the resulting local properties.

2.3. Characterization

2.3.1. Mechanical Characterization

The geometrical analysis of hat-shaped profiles is done using GOM Atos V and GOM Inspect. The angle is measured between the top and wall surface. Then, they were cut into three parts, the top and two wall parts, with a band saw type SSF/420

Table 2. Process parameters including quenching time and cooling media on the final microstructural and mechanical properties of the functionally graded parts. All conditions were subjected to an aging treatment after forming.

Sample notation	Quenching time [s]	Cooling media	Transfer time [s]
8A	8	Air	25
8W		Water	
30A	30	Air	
30W		Water	
30W-10	30	Water	10

(August Mössner KG, Schwäbisch Gmünd-Mutlangen, Germany). For hardness measurements, samples were cut from the top, flange, and wall surfaces of the hat-shaped profile via a cutting machine (Struers, Discotom 5) at different locations indicated with blue diamond (**Figure 3a**). The samples were embedded in epoxy resin and then ground with SiC emery papers (mesh sizes of 220-500-800-1000-2500-4000) and cleaned with deionized (DI) water and ethanol, respectively. A DuraScan 20 (Emco-test Prüfmaschinen GmbH) employing 1000 g load and dwell time of 30 s was used to measure the Vickers hardness.

Uniaxial tensile tests were performed at a strain rate of 0.001 s⁻¹ using a Zwick Roell 100 kN machine (ZwickRoell GmbH & Co. KG, Ulm, Germany) with a video extensometer (videoXtens). Subsize flat tensile test samples, **Figure 3b**, were cut from the top surface of the hat-shaped profile, and three samples from the heated and cold sections were used for statistical analysis.

Moreover, in situ tensile tests were performed for samples formed in the tool having a temperature of 300 °C. Those samples had similar graded properties as compared to the 30W-10 sample in terms of microstructure and hardness. For in situ tensile testing, samples with a cross section of 6 mm × 1.3 mm and a gauge length of 35 mm were used. The samples were taken from the middle section of the hat-shaped profile (**Figure 3a**). The surface was ground down to 5 μm grit size and polished utilizing a colloidal silica suspension. Subsequently, the sample was sandblasted to create a stochastically distributed pattern on the surface. Tests were conducted using an electromechanical MTS criterion Model 43 operated in displacement control with a constant crosshead speed of 0.01 mm s⁻¹. The global strain was calculated based on displacement data. A Nikon D3200 digital camera equipped with a Nikon AF-5 Micro Nikkor 105 mm objective lens was used to take the images for digital image correlation (DIC). Mechanical tests were stopped every 0.35 mm, i.e., every 1% strain. Afterward, local strain calculations were made using the software VIC 2D (Vers. 6) by Correlated Solutions.

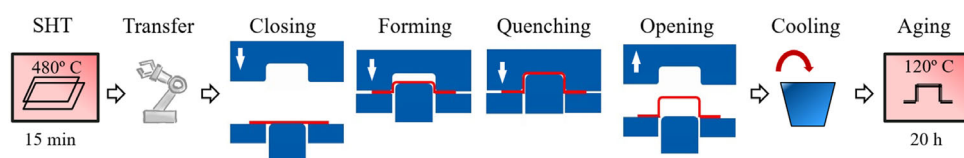


Figure 2. Schematic representation of the hot stamping process. See text for details.

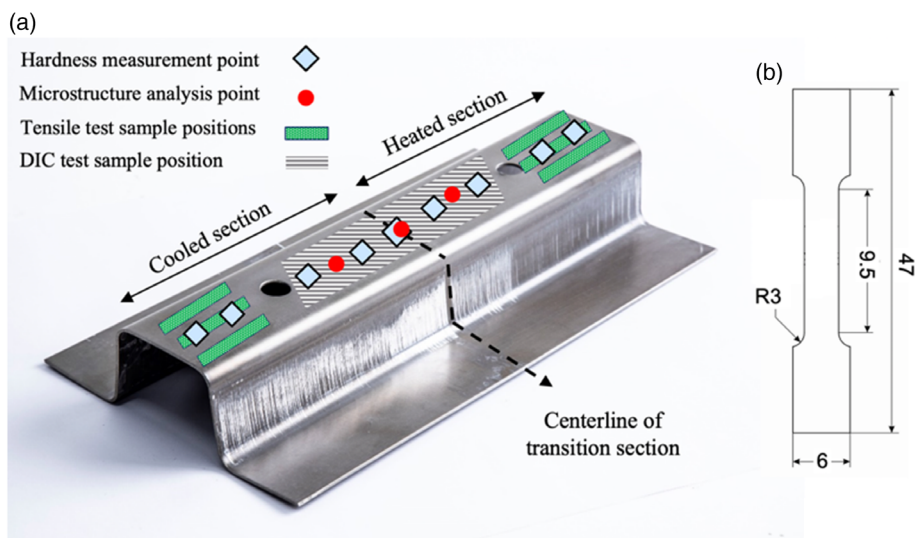


Figure 3. a) Location of tensile test samples, microstructure, hardness, and DIC measurement areas across the hat-shaped profile and b) subsize flat tensile test geometry used for tensile testing (dimensions in mm).

2.3.2. Microstructure Analysis

Microstructure characterization was performed using SEM (CamScan MV 2300) equipped with a tungsten filament at an accelerating voltage of 30 kV. Back-scattered electron (BSE) mode was employed for analyzing the second-phase particles. In order to perform electron backscatter diffraction (EBSD) analysis, cut samples were initially cut from the top surface of the hat-shaped profile (Figure 3a), and then ground and vibro-polished for 24 h in a colloidal silica solution (OPS). Fracture surface analysis was performed by a SEM (JSM6610LV, JEOL Inc.) operated at 20 kV in secondary electron (SE) mode. For phase analysis, samples were characterized using XRD employing an Empyrean four-circle diffractometer (Panalytical) with Cu $K\alpha$ radiation. The primary beam path was equipped with a poly capillary system and a double cross slit, which created a beam size of 5 mm in width and 1 mm in height. On the secondary beam path, a parallel collimator in front of a Ge monochromator was installed.

A scanning range (2θ) of 15° – 140° with a step size of 0.01° and an exposure time of 3.5 s per step was used.

The crystal structure and morphology of the samples and precipitates were analyzed by using a TEM (JEM-2100, JEOL Inc.), operating at 200 kV. Samples were disc-punched from thin foils, mechanically thinned to 10 μm , and Ar ion-etched until perforation (PIPS Mod. 691, Gatan Inc.). Micrographs were recorded by a slow-scan CCD camera (Orius SC1000, Gatan Inc.).

3. Results and Discussion

3.1. General Consideration

High-strength aluminum alloys show limited formability and, thus, pronounced springback after forming; however, a thermomechanical process is expected to reduce springback.^[5,21]

Figure 4 shows two formed geometries after the cold and hot forming–die quenching process. The target angle being 93° , the

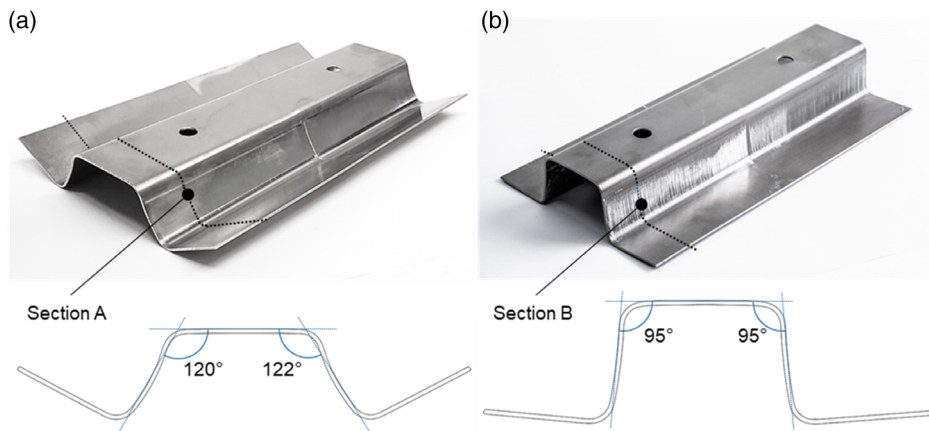


Figure 4. Hat-shaped profile of a) the formed T6-7075 alloy at room temperature and b) the hot-formed and die-quenched SHT AA7075 alloy.

T6-condition hat-shaped profile exhibits low-dimensional accuracy, Figure 4a, while the hot-formed and die-quenched SHT profile, Figure 4b, reveals almost no springback. Therefore, it can be concluded that the thermomechanical process, in which functionally graded properties are thought to be achievable by controlling the local cooling conditions during forming, enhances the dimensional accuracy of components formed out of an AA7075 alloy. In how far this really is the case will be shown and discussed in the remainder of the present article.

3.2. Impact of Quenching Conditions

3.2.1. Mechanical Characterization

Figure 5a displays the hardness distributions at the top surface of four different hat-shaped profiles, with quenching times of 8 and 30 s in the tool followed by cooling in water and air, respectively (see Table 2). Here, the transfer time from the furnace (SHT) to the tool was kept constant at 25 s. All samples are characterized by an obvious gradient in the hardness distribution, changing from a softer area within the profile area being formed in the heated tool section to a harder area in the cooled section. Therefore, graded properties are successfully obtained, with

an increase of hardness within a local transition section of about 40 mm in width.

A short quenching time and air cooling (8A) promote the least pronounced gradient. However, the water-cooled sample (8W) shows a significant increase in the overall hardness. A similar hardness distribution can be obtained with a longer quenching time and air cooling (30A). Again, water cooling increases the overall hardness with the steepest gradient up to 150 HV1 in the cooled section. The difference in hardness between sections increases from 15 HV1 (8A) up to a maximum of 35 HV1 (30W).

The medium hardness of the 8W condition shows that a quenching time of 8 s in the tool being used in the present study is not sufficient to cool down the blank sufficiently to eventually avoid unwanted precipitation before aging (leading to the evolution of relatively coarse precipitates). However, the pressure holding time in practical production cannot reach 30 s; hence, the optimization of forming tools, forming strategies, and forming processes should be considered in order to obtain superior mechanical properties even with a holding time of 8 s. However, this is beyond the scope of the present work and it will be addressed in a follow-up study.

Figure 5b reveals the influence of the tool contact areas on the hardness distribution. The middle of the transition area is

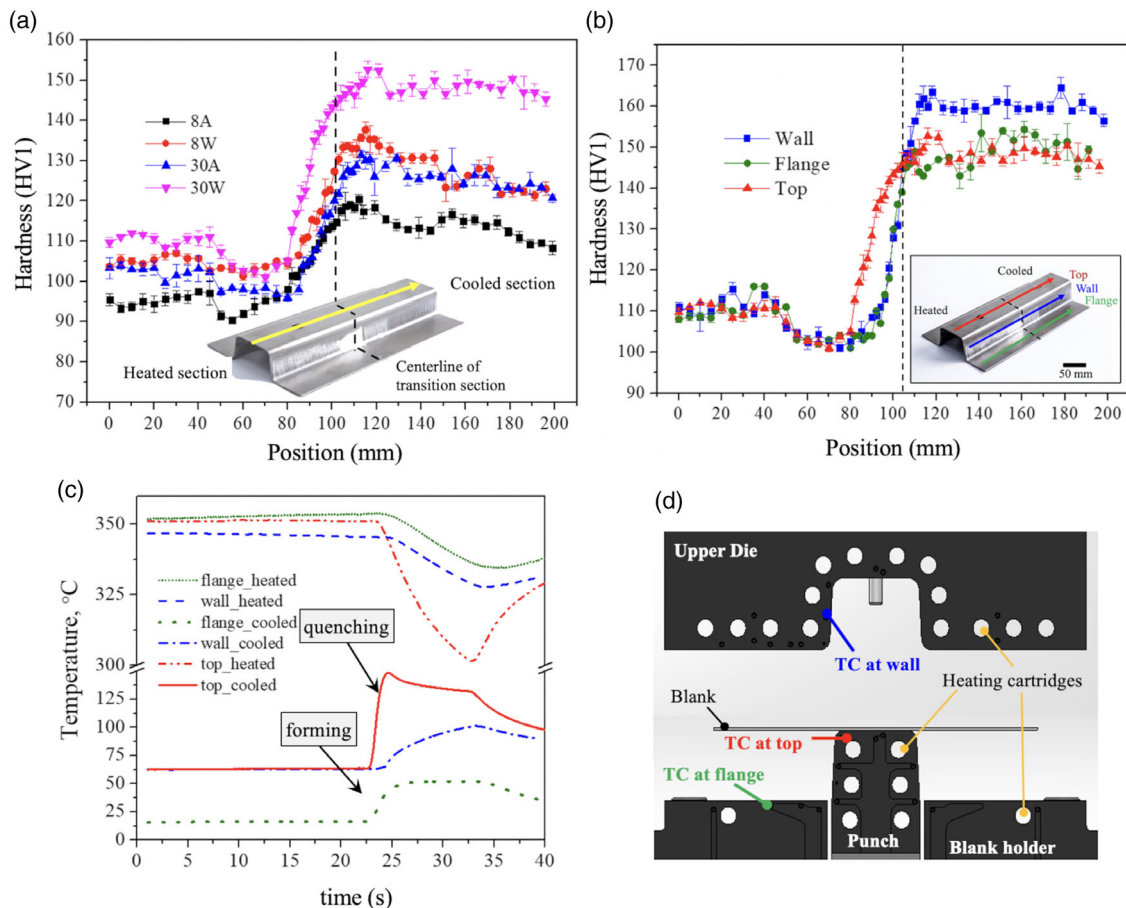


Figure 5. Hardness distribution throughout the hat-shaped profile from the heated to the cooled section a) for different conditions: 8A, 8W, 30A, and 30W samples, b) for the different sections of the 30W sample; c) temperature change at the specific section in the tool during the forming–quenching process, and d) cross section of the heated section showing the actual positions of TCs.

marked by the dashed line on both the hat-shaped profile and the hardness graph. The top surface is characterized by a sudden increase of hardness at the end of the heated section, whereas the wall and flange surfaces exhibit a more gradual increase with a sharp transition to a stable hardness level in the cooled section. The wall area reaches the highest hardness of about 160 HV1.

The changes in the hardness distribution are most likely due to different contact conditions during forming and quenching, eventually influencing the heat transfer as a result. The top surface is in contact with the punch from the direct start of forming, with forces in the forming zone pulling the top area against the punch. This leads to higher contact pressure and increased heat transfer.^[22] The result is a sudden increase in hardness from the heated section to the transition section. However, the wall and flange surfaces were only subjected to reduced contact loads. On the one hand, due to the constant distancing of 1.7 mm between both sections, the contact area and contact pressure were limited on the flange surface. On the other hand, the wall section did not touch any tool surface until the end of the forming process, eventually limiting the influence of contact-related effects until the quenching stage. However, during the quenching stage, the wall area was under high contact loads as the distance of the tool surface could reach values of less than 1.5 mm.

Taking this into account, at least partially reduced contact loads in the flange and wall surfaces reduced the heat transfer between tool and blank. This would lead to inhomogeneous tool temperatures during forming and quenching. Therefore, the temperature profile, Figure 5c, was measured using K-type TCs integrated into the die in the characteristic areas (Figure 5d). The temperature changes in both sections started after forming and remained until quenching. As expected, the temperature suddenly dropped in the heated sections and increased in the cooled sections due to the forming process and the high contact pressure and heat transfer between the blank and top surface of the punch, respectively. The reduced contact loads in the flange and wall resulted in comparatively slower quenching rates and smaller changes in tool temperature (Figure 5c). Besides, the temperature measurement for the top surface was taken at the corner of the punch and, thus, not exactly at the position where the hardness profile was determined (Figure 5b). Here, the corner of the punch is exposed to

higher contact pressure during the forming–quenching process. Thus, the most pronounced temperature change at the cooled and heated sections, respectively, was expected at this specific position only.

It should be also noted that deformation was induced in the side walls; thus, a high density of dislocations supported the evolution of the finest precipitates (heterogeneous nucleation/precipitation) upon aging in these regions. It is well known that dislocations provide for additional nucleation sites for precipitation.^[23,24] This was not the case in the heated tool, as coarse precipitates already formed before aging.

The mechanical properties obtained by tensile testing after hot forming and die quenching with various parameters are given in Figure 6. The samples formed in the cooled section of the die exhibit similar ultimate tensile (UTS) and yield strength (YS) values as compared to the as-received T6 condition, i.e., 588 and 531 MPa, respectively.^[25] Samples from the heated section show a 65% reduction in yield strength and a 75% improvement in ductility. However, the significant influence of the parameters on the hardness is less significant for the elongation (EL) values. The reason could be the formation of larger precipitates within the heated section of the tool during the hot forming–die quenching process. Sajadifar et al. also found similar results for AA7075 alloys, in which the microstructure after forming is not supersaturated like that formed on the cooled section.^[16]

The macroscopic and the local deformation behavior of the 30W-10 sample were characterized using the DIC technique (Figure 7). The sample shown was taken from the middle section of the hat-shaped profile, Figure 3a, in order to study the localized deformation patterns within the graded part. In situ tensile experiments revealed that plastic deformation is localized in that region of the graded part that was formed on the heated side of the forming tool. Already in the very early stages of deformation strain localization can be seen; however, strain induced hardening leads to the transfer of plastic deformation to the adjacent sample areas. No traces of local embrittlement are seen in the sample. The maximum strain obtained via DIC was about 16%. The spot of highest deformation is affected not only by the microstructure gradient but also by the sample geometry considered. Thus, the decrease of local strains to the right is not an effect of local microstructure but an increase of sample cross

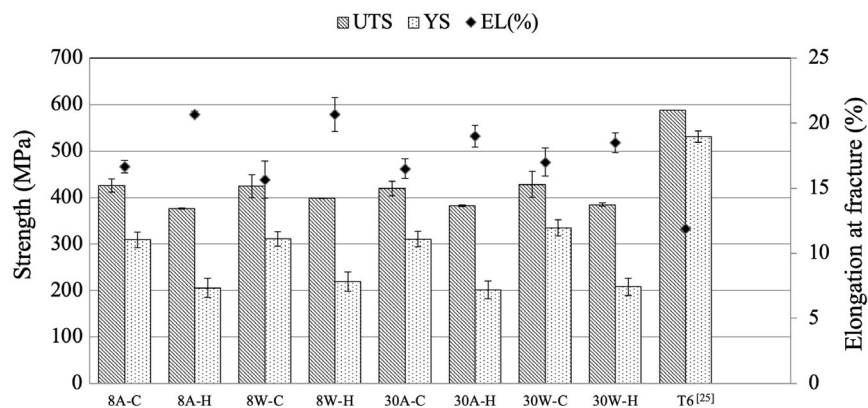


Figure 6. Mechanical properties of samples subjected to different processes. All conditions were subjected to an aging treatment after forming.

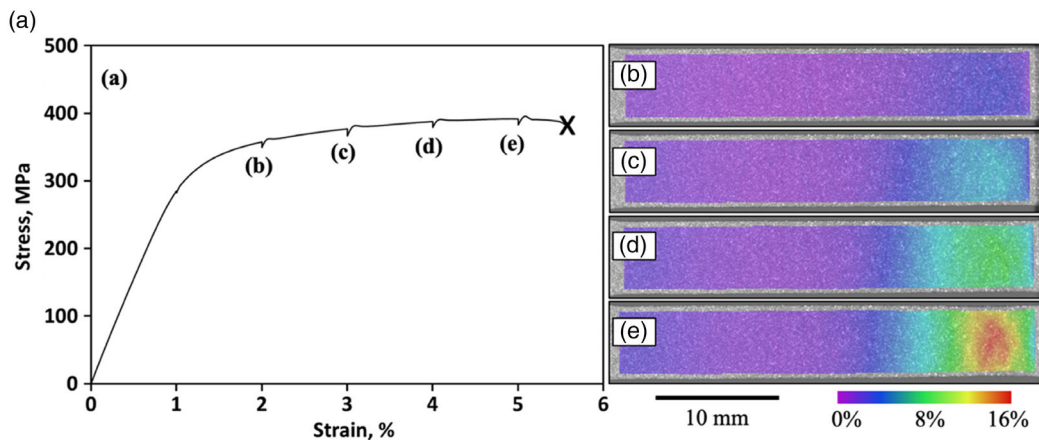


Figure 7. a) Engineering stress–strain curve of the 30W-10 sample and corresponding local strain distribution at selected global strains of b) 2%, c) 3%, d) 4%, and e) 5%.

section and minor notch effects, respectively. Evidently, lower yield strength and higher ductility of the material formed on the heated section of the tool compared to that formed on the cooled section can result in localization of deformation during the loading of the graded part. As elaborated in the following section, the formation of the second-phase particles with various sizes and morphologies is responsible for such an observation.

The fracture surfaces of the hot-formed and die-quenched AA7075 alloys after a quasistatic tensile test were analyzed via SEM to understand the effect of different tool temperatures, i.e., 350 and 25 °C. All surfaces have similar characteristics; therefore, only representative images of the sample quenched for 30 s in the tool and subsequently water cooled are given in **Figure 8**. Both fracture surfaces of samples formed in the heated and cooled section of the tool show dimples and microvoids, confirming the presence of a ductile fracture mechanism. It can be seen that the deformation within the heated section (350 °C) leads to a slightly increased size of the dimples and microvoids (**Figure 8a**). It is known that higher deformation temperatures enhanced the diffusion rate as the responsible mechanism for the coalescence of microvoids.^[18] Therefore, smaller dimples and microvoids were observed in samples deformed on the cooled section in the present study (**Figure 8b**).

3.2.2. Microstructure Analysis

For the visual assessment of second-phase particles formed during the thermomechanical treatments employed in the present study, BSE micrographs of the samples quenched in the tool for 8 and 30 s are shown in **Figure 9**. As observed, the formation of the coarse precipitates took place in the microstructures of all samples examined. According to the previous studies on the EN AW 7075 alloy,^[26,27] coarse precipitates formed are presumably η phase with a stoichiometry close to MgZn_2 . White MgZn_2 precipitates are shown with yellow arrows, encircling individual bulk grains in **Figure 9**. The formation of coarse precipitates leads to large interparticle spacing.^[28,29] As a result of large interparticle spacing, dislocation motions can occur with less resistance during further deformation/loading of the material, eventually degrading the strength and hardness of components. Low strengths and hardness values obtained for all samples (even for the sample formed for 8 s on the cooled side of the tool following water cooling) already indicate that the interparticle spacing should be relatively large.

It is also worth noting that higher volume fractions of coarse precipitates can be seen through the microstructure of the samples formed on the heated and transition sections of the tool compared to those formed within the cooled section. The low

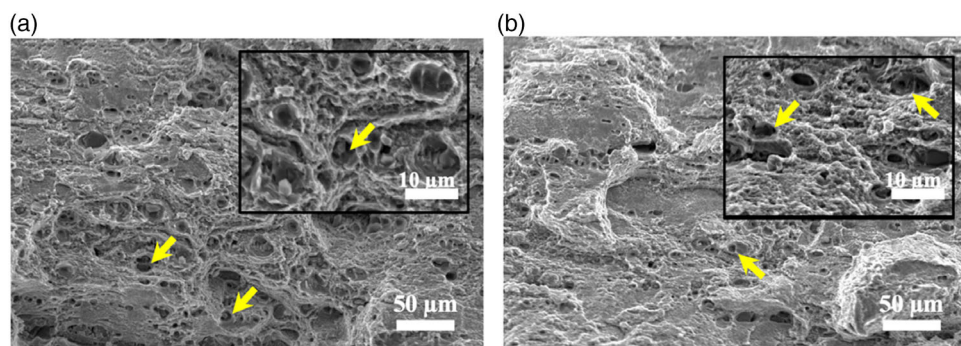


Figure 8. SEM micrographs of fracture surfaces taken from a) the heated and b) the cooled sections of the 30W sample.

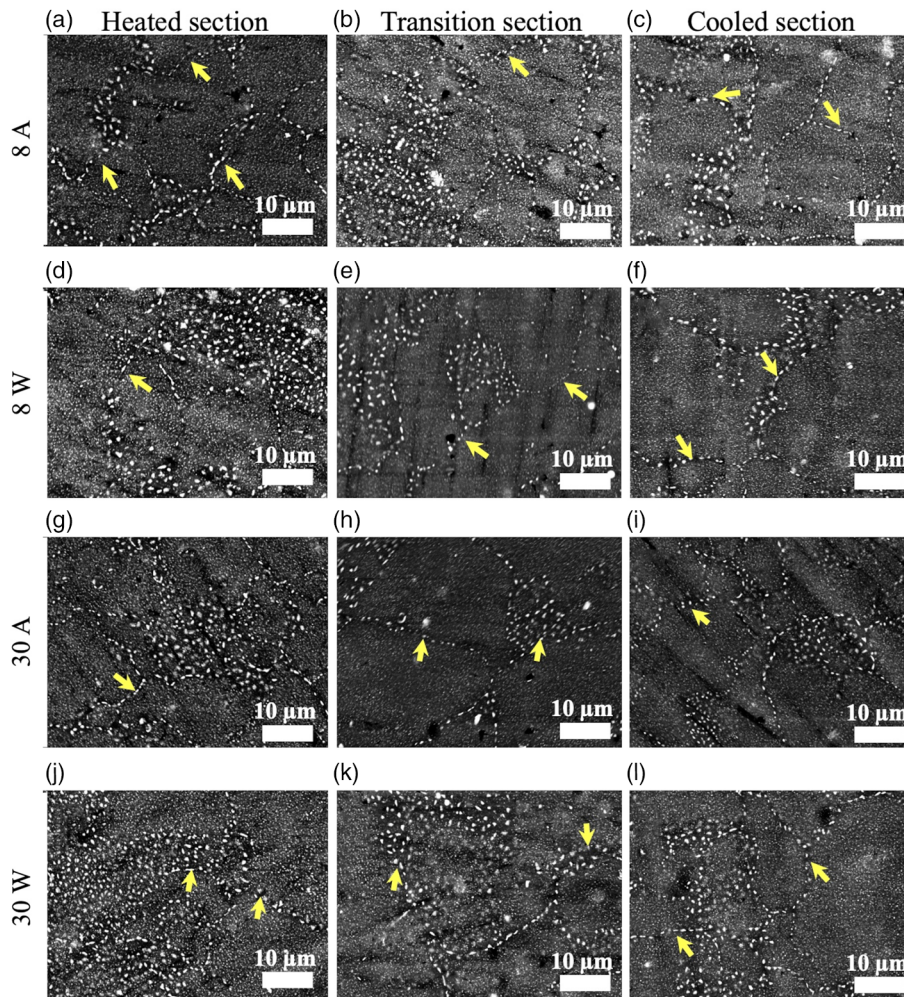


Figure 9. BSE micrographs of the a–c) 8A and d–f) 8W, g–i) 30A, and j–l) 30W samples.

cooling rate from solution heat treatment temperature within the heated and transition sections results in the formation of coarse precipitates along the grain boundaries and within the grain interior. The formation of precipitates before the aging treatment reduces the supersaturation degree of the SHT sample. Hence, during the subsequent aging treatment, the solute atoms further segregate toward coarse precipitates to assist the growth of second-phase particles formed.^[26,30]

Other important parameters to be considered are quenching time and cooling media. The characterization of the mechanical properties revealed that samples formed in the tool for 30 s followed by water quenching, resulting in the highest difference in mechanical properties between the cooled and heated sections. This can be attributed to both a higher cooling rate in water after forming and a higher contact time in the sample formed in the tool for 30 s. However, the aforementioned microstructural reasons can hardly be assessed on the basis of BSE images. The size of nanoscale precipitates can hardly be compared in the BSE micrographs shown. Due to the resolution limitation of the SEM employed, only coarse η precipitates can be distinguished. The sizes of η' precipitates and Guinier–Preston (GP) zones as

strengthening precipitates are supposed to be less than 10 nm. Therefore, SEM studies can only be used to characterize coarse precipitates formed through the microstructure. In the following section, TEM studies are carried out to characterize η' precipitates and GP zones in depth.

3.3. Impact of Transfer Time

3.3.1. Mechanical Characterization

In the hot forming–die quenching integrated process, different tool temperatures allow for tailoring the mechanical properties and the microstructure of AA7075 alloy. This can be easily correlated with the hardness profile, uniaxial tensile test, and microstructural analysis of AA7075 in the previous sections. On the other hand, the authors assumed that an even improved hardness and tensile strength in the cooled die can be obtained by a reduced transfer time, i.e., the time period between taking the blank out of the furnace and the start of the forming process. It is well known that the transfer time affects the properties and the characteristic of the transition section such that the

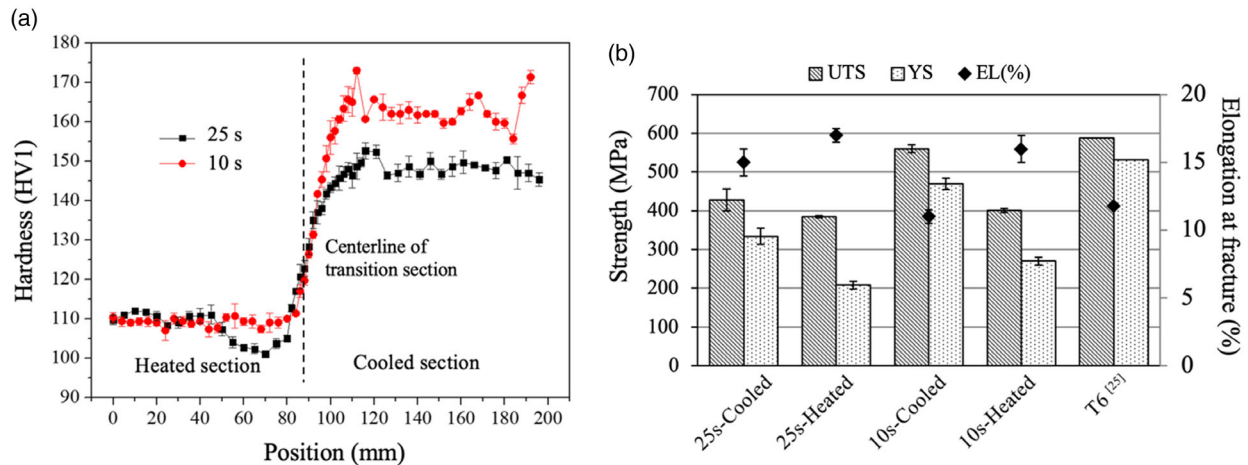


Figure 10. a) Hardness distribution and b) mechanical properties of 30W samples with 10 and 25 s transfer times.

temperature of the blank is expected to decrease during transfer time, which finally leads to a change in the quenching rate.^[25] As considerable temperature losses during the transfer of the blank can influence the material properties, a comparative study was conducted using transfer times of 25 and 10 s.

Figure 10a shows the comparison of hardness results before and after reducing the transfer time. Although a slight change was detected in the heated section, the most significant influence on the hardness is observed within the cooled section after 10 s with an increase of hardness to about 165 HV1. It can be said that the transfer time influences not only the hardness but also the characteristic of the transition section. Here, it could be revealed that the hardness gradient in the transition section is considerably higher after 10 s than after 25 s of transfer. Pronounced changes in hardness are seen just after the end of the transition section and the remaining region of the cooled section. This fact is thought to be related to inhomogeneous contact conditions between the blank and the tool.

Figure 10b reveals the effect of the transfer time on the mechanical properties of the AA7075 alloy. The influence on the yield strength of the alloy is more pronounced when the transfer time decreases from 25 to 10 s on both heated and cooled sections. As the temperature loss is expected to lessen in the case of 10 s transfer time, a more pronounced temperature gradient was maintained at the cooled section resulting in higher strength values. Obviously, the elongation decreases when the transfer is decreased to 10 s.

3.3.2. Microstructure Analysis

BSE micrographs of the sample with a transfer time of 10 s and then quenched in the tool for 30 s followed by water cooling (30W-10) are shown in Figure 11. As can be seen, coarse precipitates were formed in the grain interior and along the grain boundaries of the heated section. BSE micrographs taken from the transition and cooled sections reveal that a lower transfer time hampered the formation of precipitates. Although a few coarse precipitates are formed along the grain boundaries in the cooled section of the sample, the volume fraction of coarse η particles is considerably lower than in the sample with a transfer time of 25 s (Figure 9). The reduced transfer time maintained a higher temperature difference between blank and tool before forming, resulting in a higher cooling rate and eventually a higher degree of supersaturation prior to aging. Hence, a higher volume fraction of fine precipitates (presumably η' phase) can be formed during subsequent aging treatment. Fine and dispersed precipitates lead to a short interparticle spacing signifying dislocation-precipitate interactions.^[29,31,32] By taking changes in the mechanical properties and microstructural evolution into account, it is worth noting that with a decrease in the transfer time, the hardness and UTS values are close to the T6 condition (Figure 10b). Higher hardness, yield strength, and UTS of the sample with a transfer time of 10 s compared to that with a transfer time of 25 s can be ascribed to the higher volume fraction of fine and dispersed second-phase particles formed.

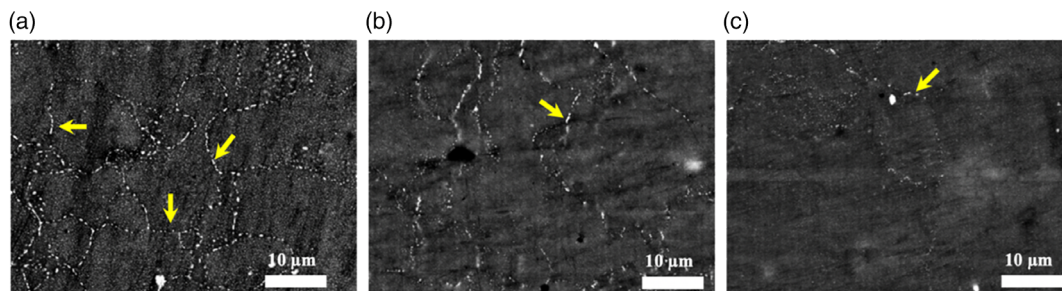


Figure 11. Backscattered SEM micrographs of the 30W-10 sample: a) heated section; b) transition section; and c) cooled section.

The type and morphology of the precipitates formed in the hot-formed and die-quenched AA7075 samples were analyzed by TEM. **Figure 12a** shows the microstructure of the sample formed in the cooled section of the tool with a small amount of coarse equilibrium η phases precipitate, and homogeneously distributed η' phase nanoprecipitates formed within the grains (**Figure 12b**). These metastable η' exhibiting a rounded platelet structure are thought to be the strengthening precipitates for AA7075 alloy.^[4,30] In addition, GP zones and needle-shaped precipitates, respectively, were observed in the microstructure of the cooled section (**Figure 12c**). Such extremely fine η' precipitates and GP zones were reported to form within the grain of AA7075 alloy after SHT and the subsequent aging process.^[27]

On the other hand, the microstructure of the heated section contains unevenly distributed coarse η precipitates both in the grain interior and at the grain boundaries (**Figure 12d–f**). As a lower cooling rate prevails in the heated section of the tool, the formation of a coarser plate-like η phase, having around 200 nm in length, was observed. Zhang et al. reported that the precipitation of η phase nucleates at grain boundaries and their amount increases with decreasing cooling rate, which is also in

agreement with the microstructural analysis of the samples.^[33] TEM studies and mechanical behavior of the graded AA7075 alloy revealed that changes in the mechanical properties throughout the graded part are related to the types and morphologies of the second-phase particles formed. The formation of fine η' precipitates and GP zones resulted in effective precipitate–dislocation interactions, eventually leading to the improvement of material strength at a loss of ductility. However, the formation of coarse η precipitates increases the interparticle spacing, eventually weakening the effect of precipitate–dislocation interactions and, hence, reducing the strength. **Figure 12g,h** depicts a detailed characterization of the GP zones. It can be concluded from the selected area electron diffraction (SAED) images that the GP zones are characterized by coherency with the Al matrix, elongated clusters seen are near-coherent (**Figure 12g**). It is well known that in Al–Zn–Mg–Cu alloys the GP zones, η' and η precipitates are coherent, semicoherent, and incoherent with the Al matrix, respectively.^[34,35] Besides, the η MgZn₂ precipitates are epitaxially intergrown in the Al matrix, elongated alongside the {111}Al plane.

XRD analysis was performed to provide an additional assessment of the second-phase particles formed during the

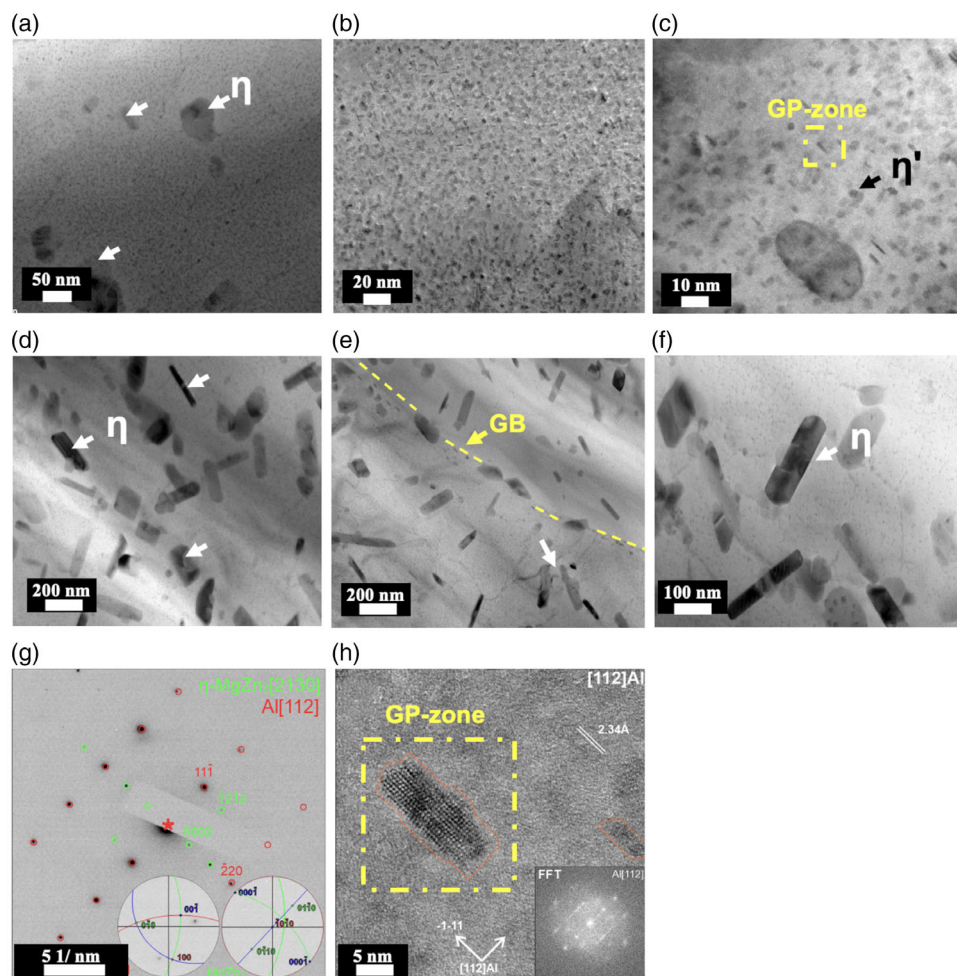


Figure 12. TEM micrographs of the 30W-10 samples formed a–c) at the cooled and d–f) heated sections of the tool. Detailed examination of GP zone of the dotted region in (c): g) experimental SAED indexed for Al (red) and η -MgZn₂ (green); insets are stereograms for both phases in corresponding orientation; h) irregular elongated near-coherent Zn–Mg clusters in the Al matrix; a fast Fourier transform (FFT) is shown in the inset.

forming/quenching sequence. **Figure 13** shows the XRD pattern for the 30A sample formed on the heated side of the tool and the 30W-10 sample with a transfer time of 10 s formed on the cooled side of the tool. The reason for choosing these two samples is to be expected the most pronounced differences between them. It is well documented that due to the overlapping peaks, the η' and η phases in the AA7075 alloy can hardly be distinguished from each other.^[36,37] XRD confirmed that second-phase particles were formed during forming and the heat treatment employed in the present study. It is also worth noting that the intensity of the peaks corresponding to η' and η phases are higher for the sample formed on the heated side of the tool compared to that formed on the cooled section. This can be ascribed to the formation of a higher fraction of coarse η precipitates in this sample (Figure 12d–f). It is well known that when the fractions of η' precipitates and GP zones are higher than that of the η phase in a sample, peaks corresponding to the second-phase particles are weaker.^[36]

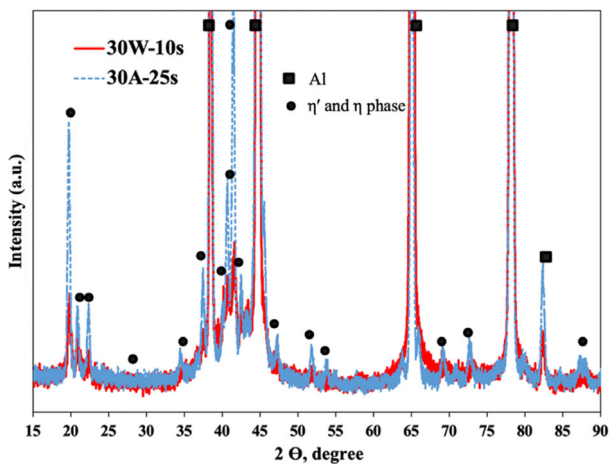


Figure 13. XRD patterns for the heated section of the 30A, and the cooled section of the 30W-10 sample.

3.4. Process–Property Relationships

The results shown in the present study revealed the ability to successfully manufacture thermomechanically processed AA7075 alloy sheets with graded properties using an active tool design. The question of how quenching and cooling rate during and after the forming process influence the precipitation kinetics and, ultimately, the property distribution of the formed hat-shaped profile was answered. Different forming–quenching times and cooling media were examined to understand the effect of various parameters on the final strengthening behavior, as well as on the achievement of a functional gradation in the AA7075 alloy.

The thermomechanical process was shown to enhance the dimensional accuracy of components formed out of a functionally graded AA7075 alloy. This was also found in the study of Maeno et al., in which an aluminum alloy part was successfully produced with high-dimensional accuracy by hot stamping.^[38] For partial heating, the tool temperature was selected as 350 °C, while room temperature was chosen within the cooled section of the tool. It was previously shown for AA7075 alloys that 350 °C is an adequate temperature to achieve a critical cooling rate for obtaining reduced strength and improved ductility in the formed part.^[16] The present study also revealed that this temperature is sufficient to establish graded properties throughout the hat-shaped profile. Moreover, different hardness distributions and, thus, a characteristic gradient behavior were observed after applying various process parameters during the hot forming–die quenching process. The water cooling after forming increased the overall hardness, finally promoting the steepest gradient in the cooled section. At the same time, no significant difference in the hardness of the heated section of hat-shaped profiles formed by various parameters was found.

The highest difference in local mechanical properties between the cooled and heated section of the hat-shaped profile is achieved by forming–quenching in the tool for 30 s followed by water cooling. The reason is thought to be a higher cooling rate in water after forming as well as a higher contact time in

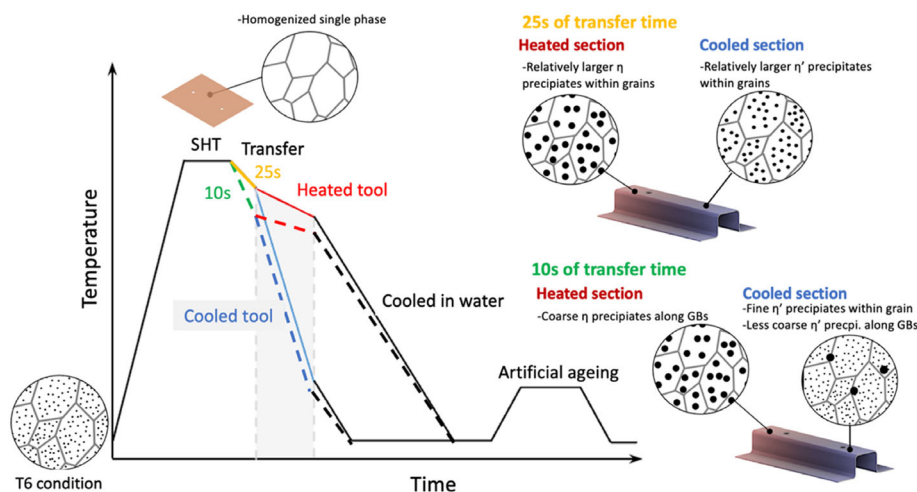


Figure 14. Schematic representation of thermomechanical process route used in the present study.

the tool during quenching. In addition, an increased contact time resulted in the extraction of more heat until the temperature of the part and the tool reached equilibrium.

A reduced transfer time affected not only the hardness but also the characteristics of the transition section in the hat-shaped profile. As a result of a less pronounced temperature loss, higher strength and lower elongation at break were attained due to a higher volume fraction of fine and dispersed second-phase particles formed in the cooled section (Figure 14). TEM investigation revealed that finely distributed precipitates (η' and GP zones) were formed at the highest cooling rates. In contrast, zones of low hardness exhibited significantly coarser η precipitates, eventually hindering precipitate–dislocation interactions, resulting in a decrease in mechanical property.

4. Conclusion

In the present study, thermomechanically processed AA7075 alloys with functionally graded properties were successfully manufactured by controlling cooling conditions, i.e., by using dies heated at 350 °C and cooled at 25 °C. This study presents comprehensive results regarding the effect of various process parameters on the strengthening behavior of high-strength aluminum alloys: 1) The hat-shaped profiles exhibit two regions after forming. The high ductility region allows for high energy absorption, while the high strength of the part can be ensured by the properties within the cooled section. Excellent structural integrity in terms of localized features can be revealed by local strain analysis employing DIC. 2) The hardness increase of samples formed within 30 s in the tool and followed by water cooling was more pronounced within the cooled section, so that the hardness level between the heated and cooled sections reached around 35 HV1 difference, leading to the formation of the most pronounced gradient in terms of mechanical properties. 3) As hot forming–quenching within the dies having different temperatures enables obtaining various cooling rates, the morphology, distribution, and size of the precipitates showed different characteristics in the cooled and heated sections of the hat-shaped profile. 4) The quenching rates inside different sections of the workpiece vary due to different contact conditions and therefore, hardness values also differ. 5) Microstructural studies based on BSE, TEM, and XRD confirmed that a high fraction of strengthening precipitates, i.e., η' precipitates and GP zones, were introduced in the section formed on the cooled side of the tool. However, a high fraction of coarse η was introduced in the section formed on the heated side of the tool. The results revealed that the gradation of AA7075 alloy through the formation of different types and morphologies of second-phase precipitates employing various forming strategies is feasible.

Acknowledgements

This work was supported by the Hessen State Ministry for Higher Education, Research and the Arts—Initiative for the Development of Scientific and Economic Excellence (LOEWE) toward conducting the ALLEGRO project (Subproject A2 and B1). The authors would like to thank Mr. Artjom Bolender and Alexander Liehr for conducting XRD measurements. J.Z. acknowledges the support of ARRS, No. P1-0417.

Open Access funding enabled and organized by Projekt DEAL.

Conflict of Interest

The authors declare no conflict of interest.

Data Availability Statement

The data that support the findings of this study are available from the corresponding author upon reasonable request.

Keywords

aluminum alloys, graded properties, hot stamping, microstructure, thermomechanical processing

Received: December 24, 2022

Revised: March 19, 2023

Published online: April 20, 2023

- [1] J. Min, F. Xie, Y. Liu, Z. Hou, J. Lu, J. Lin, *CIRP J. Manuf. Sci. Technol.* **2022**, *37*, 11.
- [2] J. Günzel, J. Hauß, C. Gaedigk, J. Bergmann, P. Groche, *IOP Conf. Ser.: Mater. Sci. Eng.* **2022**, *1238*, 012014.
- [3] X. Fan, Z. He, S. Yuan, P. Lin, *Mater. Sci. Eng., A* **2013**, *587*, 221.
- [4] Y. F. Jiang, H. Ding, M. H. Cai, Y. Chen, Y. Liu, Y. S. Zhang, *Mater. Charact.* **2019**, *158*, 109967.
- [5] B. A. Behrens, S. Hübner, H. Vogt, *IOP Conf. Ser.: Mater. Sci. Eng.* **2018**, *418*, 012027.
- [6] E. Scharifi, D. Kuhnhen, A. Ademaj, U. Weidig, in *6th Int. Conf. Hot Steel Metal Forming of High-Performance Steel, CHS2 2017-Proceedings 2017*, p. 683, ISBN: 9781935117667.
- [7] E. P. Vuorinen, A. G. Ozugurler, J. C. Ion, K. Eriksson, M. C. Somani, L. P. Karjalainen, S. Allain, F. G. Caballero, *Metals* **2019**, *9*, 357.
- [8] M. Wang, C. Zhang, H. Xiao, B. Li, R. Muvunzi, D. M. Dimitrov, S. Matope, T. M. Harms, P. Groche, R. Huber, F. Machines, K. Kusumi, J. Maki, N. Nomura, R. Muvunzi, D. M. Dimitrov, S. Matope, T. M. Harms, T. Maeno, K. I. Mori, M. Fujimoto, Y. Li, S. Li, J. He, Y. Chen, L. Yue, K. I. Mori, S. Maki, Y. Tanaka, B. T. Tang, et al., *CIRP Ann. Manuf. Technol.* **2018**, *152*, 75.
- [9] S. Ertürk, M. Sester, M. Selig, P. Feuser, K. Roll, *AIP Conf. Proc.* **2011**, *1383*, 610.
- [10] M. Merklein, M. Wieland, M. Lechner, S. Bruschi, A. Ghiotti, *J. Mater. Process. Technol.* **2016**, *228*, 11.
- [11] E. Scharifi, T. Schade, A. Ademaj, S. V. Sajadifar, U. Weidig, T. Niendorf, K. Steinhoff, *Steel Res. Int.* **2021**, *92*, 2000633.
- [12] B. T. Tang, S. Bruschi, A. Ghiotti, P. F. Bariani, *Finite Elem. Anal. Des.* **2014**, *81*, 69.
- [13] R. George, A. Bardelcik, M. J. Worswick, *J. Mater. Process. Technol.* **2012**, *212*, 2386.
- [14] E. Scharifi, S. V. Sajadifar, G. Moeini, U. Weidig, S. Böhm, T. Niendorf, K. Steinhoff, *Adv. Eng. Mater.* **2020**, *22*, 2070033.
- [15] E. Scharifi, M. Roscher, S. Lotz, U. Weidig, E. Jäggle, K. Steinhoff, *Key Eng. Mater.* **2021**, *883*, 159.
- [16] S. V. Sajadifar, E. Scharifi, U. Weidig, K. Steinhoff, T. Niendorf, *HTM J. Heat Treat. Mater.* **2020**, *75*, 177.
- [17] E. Scharifi, R. Knoth, U. Weidig, *Procedia Manuf.* **2019**, *29*, 481.
- [18] S. V. Sajadifar, E. Scharifi, U. Weidig, K. Steinhoff, T. Niendorf, *Metals* **2020**, *10*, 884.
- [19] N. Rigas, M. Jäckisch, M. Merklein, *Proc. Inst. Mech. Eng., Part B: J. Eng. Manuf.* **2022**, 095440542211351, <https://doi.org/10.1177/09544054221135114>.

- [20] E. Scharifi, J. R. Mianroodi, M. Roscher, U. Weidig, E. A. Jäggle, K. Steinhoff, *Mater. Lett.* **2023**, 331, 133465.
- [21] B. A. Behrens, F. Nürnberger, C. Bonk, S. Hübner, S. Behrens, H. Vogt, *J. Phys. Conf. Ser.* **2017**, 896, 012004.
- [22] L. Ying, T. Gao, M. Dai, P. Hu, *Investigation of Interfacial Heat Transfer Mechanism for 7075-T6 Aluminum Alloy in HFQ Hot Forming Process*, Elsevier, Amsterdam **2017**.
- [23] H. Hargarter, M. T. Lyttle, E. A. Starke, *Mater. Sci. Eng., A* **1998**, 257, 87.
- [24] S. V. Sajadifar, P. Krooß, H. Fröck, B. Milkereit, O. Kessler, T. Niendorf, *Metals* **2021**, 11, 1142.
- [25] J. Günzel, J. Hauß, *IOP Conf. Ser.: Mater. Sci. Eng.* **2021**, 1157, 012086.
- [26] E. Scharifi, U. Savaci, Z. B. Kavaklioglu, U. Weidig, S. Turan, K. Steinhoff, *Mater. Charact.* **2021**, 174, 111026.
- [27] R. Goswami, S. Lynch, N. J. H. Holroyd, S. P. Knight, R. L. Holtz, *Metall. Mater. Trans. A* **2013**, 44, 1268.
- [28] S. V. Sajadifar, E. Scharifi, T. Wegener, M. Krochmal, S. Lotz, K. Steinhoff, T. Niendorf, *Int. J. Fatigue* **2022**, 156, 106676.
- [29] H.-J. Christ, H. Mughrabi, *Fatigue Fract. Eng. Mater. Struct.* **1996**, 19, 335.
- [30] J. Buha, R. N. Lumley, A. G. Crosky, *Mater. Sci. Eng., A* **2008**, 492, 1.
- [31] H.-J. Christ, K. Lades, L. Volkl, H. Mughrabi, *Low Cycle Fatigue and Elasto-Plastic Behaviour of Materials-3*, Vol. 1, Springer, Dordrecht **1967**, p. 5.
- [32] S. V. Sajadifar, G. Moeini, E. Scharifi, C. Lauhoff, S. Böhm, T. Niendorf, *J. Mater. Eng. Perform.* **2019**, 28, 5255.
- [33] Y. H. Zhang, S. C. Yang, H. Z. Ji, *Trans. Nonferrous Met. Soc. China* **2012**, 22, 2087.
- [34] G. Sha, A. Cerezo, *Acta Mater.* **2004**, 52, 4503.
- [35] J. Luo, H. Luo, S. Li, R. Wang, Y. Ma, *Mater. Des.* **2020**, 187, 108402.
- [36] K. Ma, H. Wen, T. Hu, T. D. Topping, D. Isheim, D. N. Seidman, E. J. Lavernia, J. M. Schoenung, *Acta Mater.* **2014**, 62, 141.
- [37] T. Aoba, M. Kobayashi, H. Miura, *Mater. Sci. Eng., A* **2017**, 700, 220.
- [38] T. Maeno, K. Ichiro Mori, R. Yachi, *CIRP Ann. Manuf. Technol.* **2017**, 66, 269.